Solar Energy Materials & Solar Cells 95 (2011) 2610–2615

Contents lists available at ScienceDirect

Solar Energy Materials & Solar Cells

journal homepage: www.elsevier.com/locate/solmat

Angle-resolved characteristics of silicon photovoltaics with passivated conical-frustum nanostructures

Ping-Chen Tseng [a], Peichen Yu [a,*], Hsin-Chu Chen [a], Yu-Lin Tsai [a], Hao-Wei Han [a], Min-An Tsai [b], Chia-Hua Chang [a], Hao-Chung Kuo [a]

[a] Department of Photonics and Institute of Electro-Optical Engineering, National Chiao Tung University, Hsinchu 30010, Taiwan, ROC
[b] Department of Electro-Physics, National Chiao Tung University, Hsinchu 30010, Taiwan, ROC

ARTICLE INFO

Article history:
Received 31 August 2010
Received in revised form
28 April 2011
Accepted 4 May 2011
Available online 26 May 2011

Keywords:
Passivation
Nanostructure
Angle-resolved reflectance

ABSTRACT

Passivation plays a critical role in silicon photovoltaics, yet how a passivation layer affects the optical characteristics of nano-patterned surfaces has rarely been discussed. In this paper, we demonstrate conical-frustum nanostructures fabricated on silicon solar cells using polystyrene colloidal lithography with various silicon–nitride (SiN_x) passivation thicknesses. The omnidirectional and broadband antireflective characteristics were determined by utilizing angle-resolved reflectance spectroscopy. The conical-frustum arrays with a height of 550 nm and a SiN_x thickness of 80 nm effectively suppressed the Fresnel reflection in the wavelength range from 400 to 1000 nm, up to an incidence angle of 60°. As a result, the power conversion efficiency achieved was 13.39%, which showed a 9.13% enhancement compared to that of a conventional KOH-textured silicon cell. The external quantum efficiency measurements confirmed that the photocurrent was mostly contributed by the increased optical absorption in the near-infrared. The angular cell efficiencies were estimated and showed improvements over large angles of incidence.

1. Introduction

Enhancing the power conversion efficiency of crystalline silicon (c-Si) solar cells has been a focus of attention over the past few decades. In order to improve light harvesting in solar cells, it is mandatory to minimize the Fresnel reflection at the air/silicon interface for the range of the entire solar spectrum. Moreover, to achieve reasonable optical absorption throughout the entire day, an angle-independent antireflection property is also desirable as in a perfect omnidirectional antireflective structure. Both topics have been the subject of intensive research for solar cells. In the past, a multilayer antireflection coating (ARC) was commonly used to reduce surface reflection. However, issues related to material selection, thermal mismatch, and instability of the thin-film stacks remained major obstacles to the application of such broadband and angle-independent antireflection coatings in solar cells [1]. Several studies of sub-micrometer gratings (SMG) on c-Si surfaces have shown ultra-low reflectivity at normal incidence and low reflectivity at large angles of incidence (AOI) for a single wavelength only [2–5]. Regardless, the angle-resolved spectral reflectance of nano-patterned surfaces had yet been investigated for silicon photovoltaics. Moreover, previous researches have suggested that sharp nanostructures, such as nano-cones or pyramids, exhibit broadband and omnidirectional antireflective properties [6–14]. However, sharp nano-tips may not be ideal in photovoltaics as they substantially result in surface states that trap photo-generated carriers and also increase challenges in making ohmic contacts for electrodes. Since a passivation layer is mandatory for solar cells, its existence also alters the optical reflection characteristics of nanostructures [15–18]. To our knowledge, there are few works that have described the characteristics of silicon solar cells with passivated SMG nanostructures. In this work we investigate the reflective characteristics and angular efficiencies of solar cells with SiN_x-passivated, flat-top SMG nanostructures, which arrange into conical-frustum arrays. The passivated nanostructures not only inhibit broadband reflectivity at a large AOI but also benefit the ohmic contacts for electrodes. The resulting power conversion efficiency achieved was 13.39%, which showed a 9.13% enhancement compared to that of a conventional KOH-textured silicon cell [19]. The external quantum efficiency measurements also confirmed that the photocurrent was mostly contributed by the increased optical absorption in the near-infrared. The short-circuit current density is enhanced from 29.32 to 32.46 mA/cm^2.

2. Methods

Polystyrene (PS) colloidal lithography was adopted to facilitate scalable fabrication of periodic nanostructures [20,21]. Self-assembled

* Corresponding author.
E-mail address: yup@faculty.nctu.edu.tw (P. Yu).

0927-0248/$ - see front matter © 2011 Elsevier B.V. All rights reserved.
doi:10.1016/j.solmat.2011.05.010

PS nano-spheres were used as sacrificial masks to fabricate sub-wavelength conical-frustum structures. During fabrication, we first spread nano-spheres with a diameter of 600 nm on a p-type c-Si substrate by adjusting the speed of the spin coater (800–3600 rpm) and the surfactant concentration. The Si wafer is 200 μm in thickness and the resistivity is in the range of 0.5–3 Ω cm. The c-Si substrate covered with a monolayer of PS spheres was subsequently etched using reactive ion etching (RIE, Samco RIE-10NR) with a RF power of 350 W, a bias power of 50 W, and a gas flow rate of $Cl:O_2=10:1$ for 70, 150, and 200 s under a pressure of 5 mtorr, which resulted in conical-frustum arrays with heights of 110, 390, and 550 nm from the surface, respectively [22]. Thereafter, the leftover PS spheres were removed by dipping the substrate into acetone with sonification for 5 min. We note that a longer etching time was also experimented with under the same conditions, which resulted in several random spikes on the top of the conical-frustum arrays due to the poor sustainability of PS spheres and therefore was not adopted. The schematic illustration and the scanning electron microscopic (SEM) image of fabricated conical-frustum arrays with various heights are shown in Fig. 1. The fabricated conical-frustum nanostructures showed a base tilt angle of 79°.

The KOH-textured cell was prepared using a p-type Si ⟨1 0 0⟩ wafer etched by a potassium hydroxide solution ($KOH:H_2O=1:1$) at 80 °C for 40 min for saw damage etch and texture etch. The microscale surface textures formed a tilted angle of ~50.5° with respect to the horizontal plane. Next, both the micro- and nano-textured substrates were doped using phosphorus oxychloride ($POCl_3$) as the diffusion source to form an n-type layer, ~200 nm deep from the surface. After the removal of the phosphosilicate glass (PSG) layer from the substrate surface with diluted hydrofluoric (HF) acid, a silicon nitride (SiN_x) layer was deposited to passivate the surface. Since the deposition of SiN_x on the conical-frustum arrays alters the spectral and angular responses of optical reflection, we investigated the reflective spectra of conical-frustum arrays with 40, 80 , and 120 nm-thick SiN_x at normal and oblique incident angles. The deposition of SiN_x was achieved using a plasma-enhanced chemical vapor deposition (PECVD, Samco PD-220NA) system with a RF power of 35 W under the controlled pressure of 100 Pa at 300 °C [23]. The gas flow rates for SiN_4, NH_3, and N_2 were 20, 10, and 490 sccm, respectively, and the growth rate was controlled at 10 nm per minute. The front and back metalization were screen-printed with conductive pastes using a semi-automatic printer (ATMASC 25PP). The electrode co-firing step was performed in a fast-firing belt furnace at a peak temperature of 800 °C. Finally, the edge isolation was achieved using a 532 nm Nd:YAG laser. Each cell was prepared with a size of 2 cm × 2 cm segmented from a 6 in. wafer.

The optical measurement was performed using an integrating sphere to collect the scattered photons, which was then analyzed by a spectrometer. The angle-resolved reflectance spectroscopic system utilized a custom-built 15 cm-radius integrating sphere with a motor-controlled rotational sample stage in the center and a broadband 300 W Xenon lamp. The collected reflectance photons were then analyzed by a spectrometer (SPM-002-ET, Photon-control Inc.) to obtain the reflective spectrum with respect to different AOIs. The system was calibrated by the reflective spectrum of a NIST-standard, intrinsic Si at normal incidence.

Efficiency measurements were performed closely following the procedure described in the international standard CEI IEC 60904-1. Both the solar cells and the reference cell were characterized under a simulated Air Mass 1.5, Global (AM1.5G) illumination [24] with a power of 1000 W/m^2. The temperature was actively controlled during the measurements and was 25 ± 1 °C. The power conversion efficiency (PCE) measurement system was consisted of a power supply (Newport 69920), a 1000 W Class A solar simulator (Newport 91192A) with a Xenon lamp (Newport 6271A) and an AM1.5G filter (Newport 81088A), a probe stage, and a source-meter with a 4-wire mode (Keithley 2400). In the calibration report by Newport Corporation, the temporal instability was 0.88%, and the non-uniformity was 0.79%. The spectrum of the solar simulator was measured by a calibrated spectradiometer (Soma S-2440) in the wavelength range from 300 to 1100 nm. Before measurement, the intensity of the solar simulator was calibrated by a mono-crystalline silicon reference cell with a 2 cm × 2 cm illumination area (VLSI Standards, Inc.) [25]. The mismatch factor (M) for the conical-frustum cell and the KOH cell were 1.009 and 0.996,

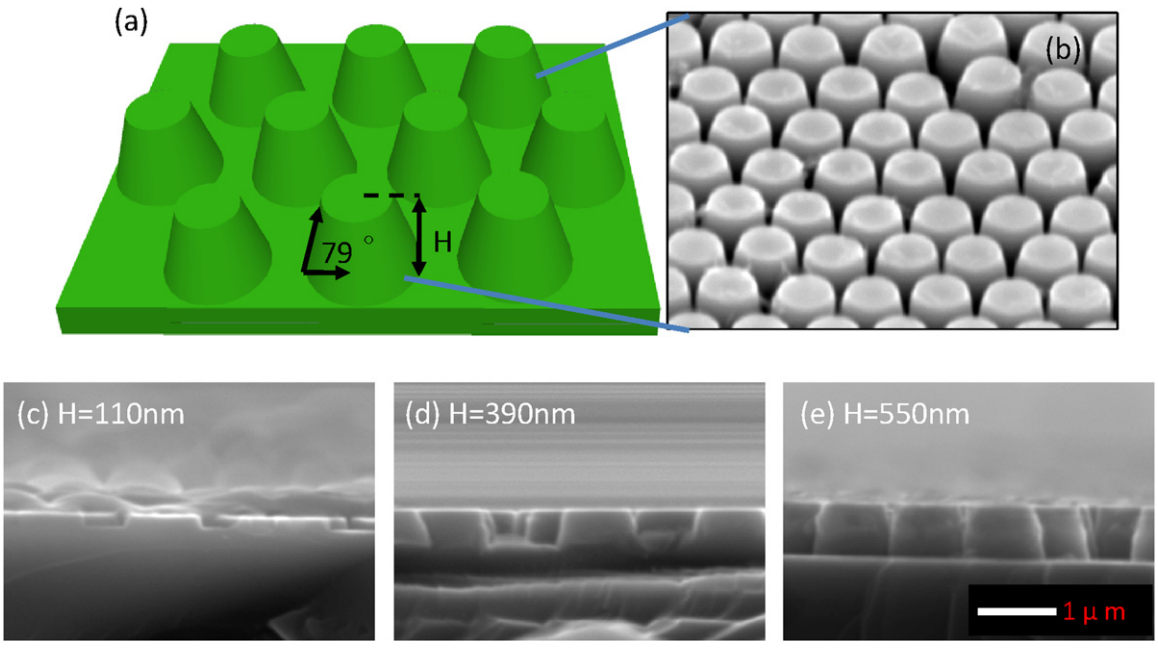

Fig. 1. (a) Schematic of conical-frustum nanostructures. (b) The scanning electron microscopic (SEM) image of conical-frustum arrays (top view) before the SiN_x deposition and the side view of conical-frustum arrays with heights of (c) 110 nm, (d) 390 nm, and (e) 550 nm.

respectively, calculated using the spectral response of the reference cell and the cell under test, the spectrum of the solar simulator, and the ASTM G173-03 reference spectrum [26].

The external quantum efficiency (EQE) system employed a 300 W Xenon lamp (Newport 66984) light source and a monochromator (Newprot 74112). The beam spot at the sample was rectangular, measuring roughly 1 mm × 3 mm. A calibration was performed using a calibrated silicon photodetector with a reported spectral response (Newport 818-UV). The EQE measurement was carried out using a lock-in amplifier (Standard Research System, SR830), an optical chopper unit (SR540) operated at 260 Hz chopping frequency, and a1 Ω resistor in shunt connection to convert the photocurrent to voltage. The temperature of cells was actively controlled during the measurements at 25 ± 1 °C.

3. Results and discussion

As shown in Fig. 2, the measured reflectance spectra of conical-frustum arrays with heights of 110, 390, and 550 nm are compared with a flat Si substrate at normal incidence. The arrays with a height of 550 nm show the best reflectivity suppression (~30%). However, without passivation, the significant surface states on the nano-textured surface could considerably hinder the current extraction. Therefore, a SiN_x layer was deposited on the arrays with a height of 550 nm not only to passivate the nano-textured surface but to further minimize the surface reflection. In Fig. 3, the measured reflectance spectra for conical-frustum arrays covered with SiN_x of various thicknesses are compared to those of a flat silicon substrate and KOH-textured silicon passivated with 80 nm-thick SiN_x at normal incidence. As shown in Fig. 3, the deposition of SiN_x drastically reduced the optical reflectivity, compared to that of bare conical-frustum arrays. With a 40 nm-thick SiN_x layer, the reflectance spectrum in the wavelength range of 400 nm $< \lambda <$ 720 nm was inhibited, whereas it remained approximately the same in the range of 720 nm $< \lambda <$ 1000 nm as the bare reference. The reflectance spectrum of 80 nm-thick SiN_x showed outstanding antireflective properties over the entire spectrum, particularly in the range of 500 nm $< \lambda <$ 600 nm (R~2%), allowing the harness of most solar power. The 120 nm-thick SiN_x only sufficiently suppressed the reflectivity in the range of 700 nm $< \lambda <$ 1000 nm ($R < 5\%$), whereas the reflectivity remained relatively high in the short wavelength range (R~20%). Overall, the addition of SiN_x passivation facilitated the optical transmission while a proper

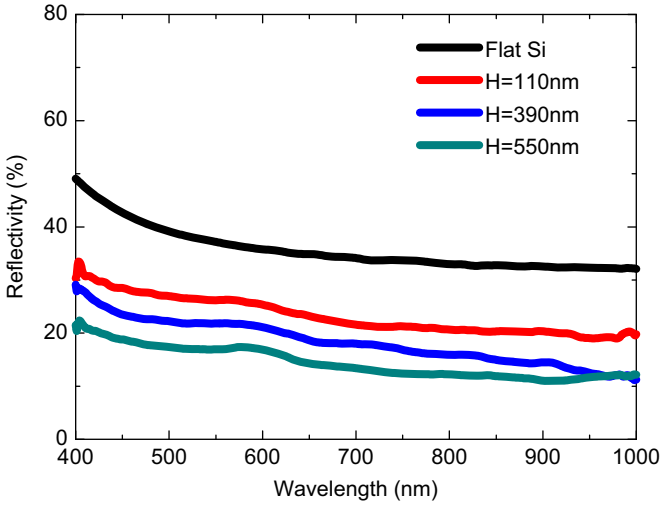

Fig. 2. Measured reflectance spectra at normal incidence of flat silicon and conical-frustum arrays with various heights.

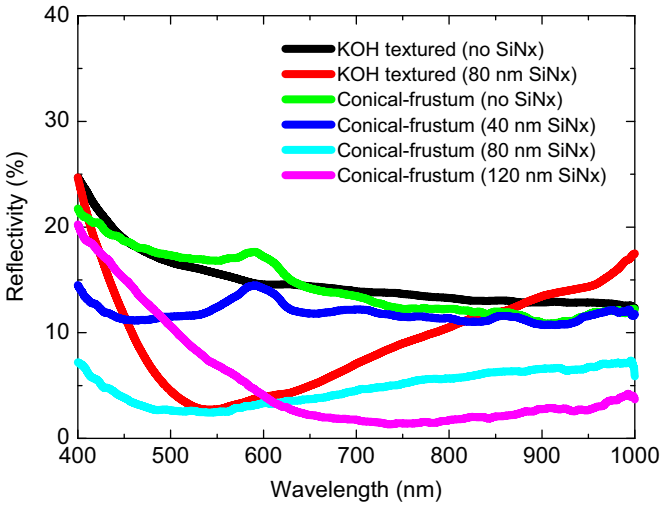

Fig. 3. Measured reflectance spectra at normal incidence of bare conical-frustum arrays, conical-frustum arrays covered with SiN_x of various thicknesses, and KOH-textured Si with 80 nm-thick SiN_x.

thickness of SiN_x could sufficiently suppress the reflectivity over the entire spectrum.

To compare the capability of solar power harvest for an entire day, a solar-spectrum (AM1.5G) weighted reflectance was defined to express the antireflective power of the nanostructures as the following:

$$\langle R \rangle = \frac{\int_{400\,\mathrm{nm}}^{1000\,\mathrm{nm}} R(\lambda) I_{AM1.5}(\lambda) d\lambda}{\int_{400\,\mathrm{nm}}^{1000\,\mathrm{nm}} I_{AM1.5}(\lambda) d\lambda} \quad (1)$$

where $R(\lambda)$ is the measured reflectivity and $I_{AM1.5}$ is the photon flux density of AM1.5G solar spectrum. The weighted reflectance $\langle R \rangle$ for no SiN_x and 40, 80, and 120 nm-thick SiN_x calculated from the measurements were 15.67%, 12.65%, 4.2%, and 7.69%, respectively.

The measured angular-reflective spectra for the KOH-etched Si, KOH-etched Si with 80 nm-thick SiN_x passivation, as well as the conical-frustum arrays 550 nm in height with no SiN_x, 40, 80, and 120 nm-thick SiN_x are shown in Fig. 4(a) (i)–(vi), respectively. The reflectivity of the bare conical-frustum arrays and those with 40 nm-thick SiN_x remained low at a small AOI and gradually increased when approaching a large AOI. Large-area omnidirectional antireflective structures are very beneficial to photovoltaic devices. We have demonstrated that the conical-frustum nanostructures not only inhibited the broadband reflectivity for normal incidence but also reduced the angular-reflective spectrum. The nanostructures covered with 80 nm-thick SiN_x showed the most inhibited reflectivity over the entire spectrum from 400 to 1000 nm and an AOI of up to 60°.

To analyze the experimental results, the weighted reflectance, $\langle R \rangle$, was employed to illustrate the angle-dependent antireflective characteristics of the nanostructures. The weighted reflectance as a function of AOI is shown in Fig. 4(b) for conical-frustum arrays covered with various SiN_x thicknesses. With the increase of AOI, the weighted reflectance of KOH-etched silicon rose more rapidly and was higher than the bare conical-frustum nanostructures. Also the KOH-etched silicon presented large variations in reflectivity for different AOIs, compared to the nanostructures. This observation indicates that the multiple surface reflections induced by KOH-etched microscale textures were not sufficient to suppress reflection at large incident angles. On the other hand, the nanoscale conical-frustum arrays showed less dependency on the AOI than the micro-textures. Still, the weighted reflectivity of

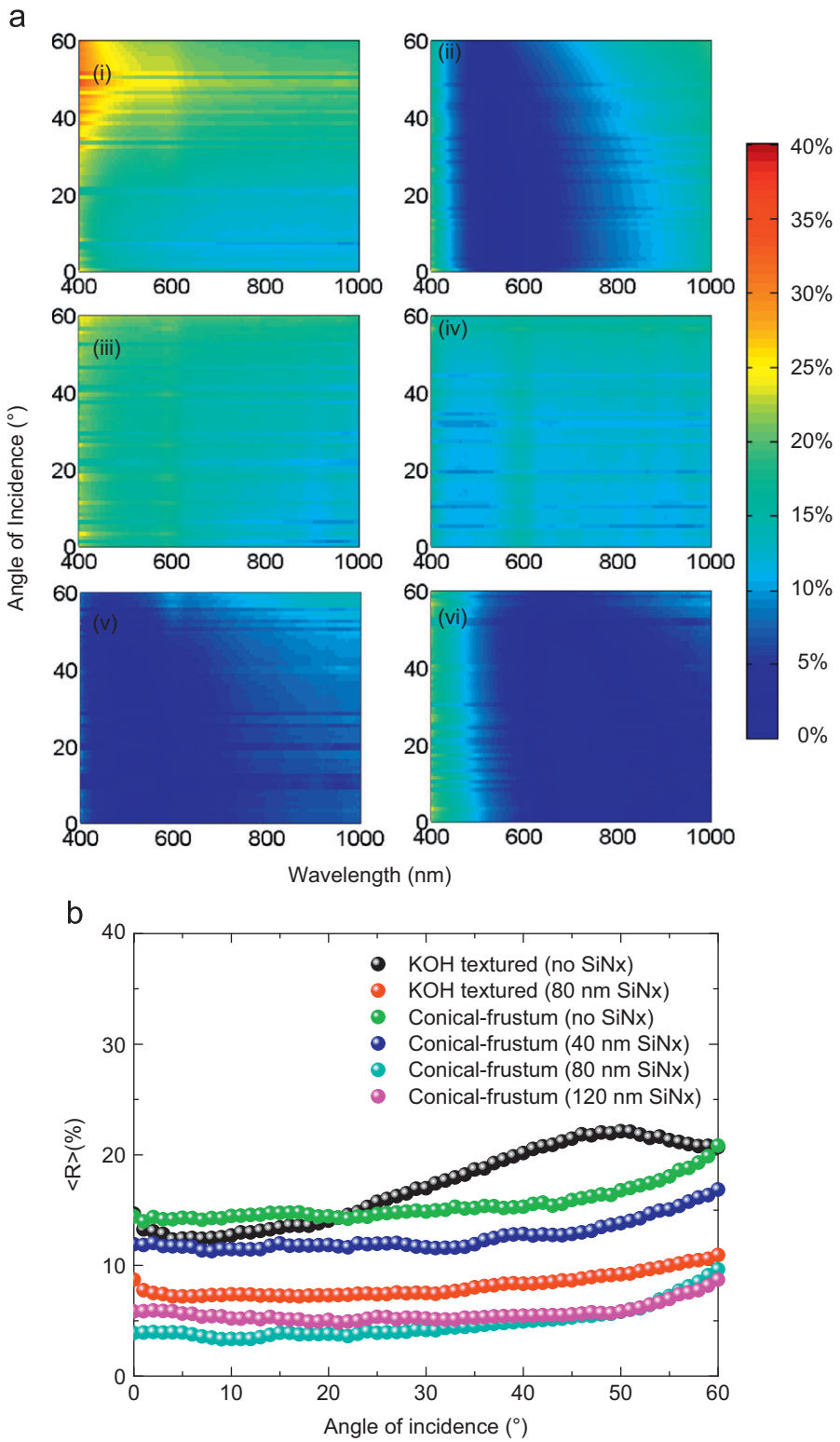

Fig. 4. (a) Measured angle-resolved reflective spectra of (i) KOH-etched silicon, (ii) KOH-etched Si with 80 nm-thick SiN_x passivation, (iii) bare conical-frustum arrays, and passivated conical-frustum arrays with SiN_x thicknesses of (iv) 40 nm, (v) 80 nm, and (vi) 120 nm. (b) The AM1.5G-weighted reflectance with respect to the angle of incidence for bare conical-frustum arrays, conical-frustum arrays with various SiN_x thicknesses, KOH-etched Si and KOH-etched Si with 80 nm-thick SiN_x.

bare conical-frustum arrays is relatively high, ~15% without a SiN_x passivation layer. As shown in Fig. 4(b), the deposition of a SiN_x layer further reduced the angular reflectance of the nano-patterned surfaces compared to that of bare structures. From the experimental results, the optimal omnidirectional antireflective properties were achieved when the conical-frustum arrays were covered with 80 nm-thick SiN_x. On average, the weighted reflectance with respect to all angles was reduced by ~10% compared to that of bare conical-frustum arrays. The weighted reflectance is as low as 4.2% for normal incidence and $<9.5\%$ up to an AOI of 60°, while the passivated KOH-etched c-Si exhibited ~10% weighted reflectance at large AOI. These results show that the conical-frustum

arrays with an 80 nm-thick SiN_x passivation layer have better omnidirectional antireflective properties than KOH-textured c-Si with the same SiN_x passivation.

The solar cell characteristics for the KOH-textured silicon and the conical-frustum arrays, both with 80 nm-thick SiN_x passivation, are listed in Table 1. The measurement was performed under a simulated AM1.5G condition with the calibration procedure described above. Six samples were respectively prepared for each type of solar cells. Table 1 shows the averages of each measurement with confidence intervals calculated from a 99% confidence level. Evidently, the optimized cell with conical-frustum nanostructures shows a superior power conversion efficiency compared to a conventional KOH-etched Si solar cell. The power conversion efficiency achieved was 13.39%, showing a 9.13% improvement over the 12.27% of the reference. Moreover, the external quantum efficiencies (EQE) of the cells were measured, as shown in Fig. 5(a). Compared to the KOH-textured silicon cell, the suppressed reflectivity at the short wavelength region ($\lambda < 600$ nm, re-plotted from Fig. 3) for the conical-frustum arrays is not evident in the EQE enhancement, possibly arising from the formation of ohmic contacts or the quality of SiN_x passivation on the nano-patterned surface, which requires further investigation. The EQE enhancement in the long wavelength range resulted from the transmission enhancement due to the passivated conical-frustum structure, since the absorption takes place at bulk, instead of the surface. Overall, the cell efficiency for the conical-frustum arrays with 80 nm-thick SiN_x passivation was much improved compared to that of the KOH-textured cell.

With the measured angle-resolved reflectance spectroscopy, the angle-dependent power conversion efficiency, η, was further estimated using the following equation:

$$\eta(\theta) = F.F. \times V_{oc} \times \frac{e}{hc} \int_{400\,\mathrm{nm}}^{1000\,\mathrm{nm}} IQE \times [1-R(\lambda)] I'_{AM1.5}\, d\lambda, \quad (2)$$

where θ is the AOI with respect to the surface normal, e is the electric charge, h is Plank's constant, c is the speed of light, and $F.F.$ and V_{oc} are the fill factor and open voltage of the cell taken from the experimental data, respectively. $I'_{AM1.5}$ is the normal component of the incident photon flux density, i.e. $I_{AM1.5}\cos(\theta)$. Internal quantum efficiency (IQE) was taken into account using the experimental data, i.e. $IQE(\lambda) = EQE(\lambda)/(1-R(\lambda))$. As shown in Fig. 5(b), the cell efficiency of passivated conical-frustum arrays remained superior to the KOH-textured Si cell up to an AOI of 49°. Moreover, an optimal cell efficiency was found at the AOI of 2° for the conical-frustum arrays by taking into account the device response to the solar spectrum. Although the calculated angular efficiencies were slightly underestimated due to the limited wavelength range (400–1000 nm) from the measured reflectance spectra, the phenomenal efficiency enhancement with respect to all AOI is promising for practical solar cell applications.

Finally, to compare the present device with previously reported solar cells, several techniques used to texture Si surfaces have shown reasonable internal quantum efficiencies for fabricated devices [27,28]. In this work, the IQE of the solar cell with an optimized conical-frustum nanostructure is better than most other light trapping structures, such as porous Si and Si nanowires, and comparable to that of an ultrafast laser textured cell. However, the conventional cells overall exhibit a better IQE response than the nano-textured cells in the short wavelength range due to a better surface passivation condition for micro-scaled textures.

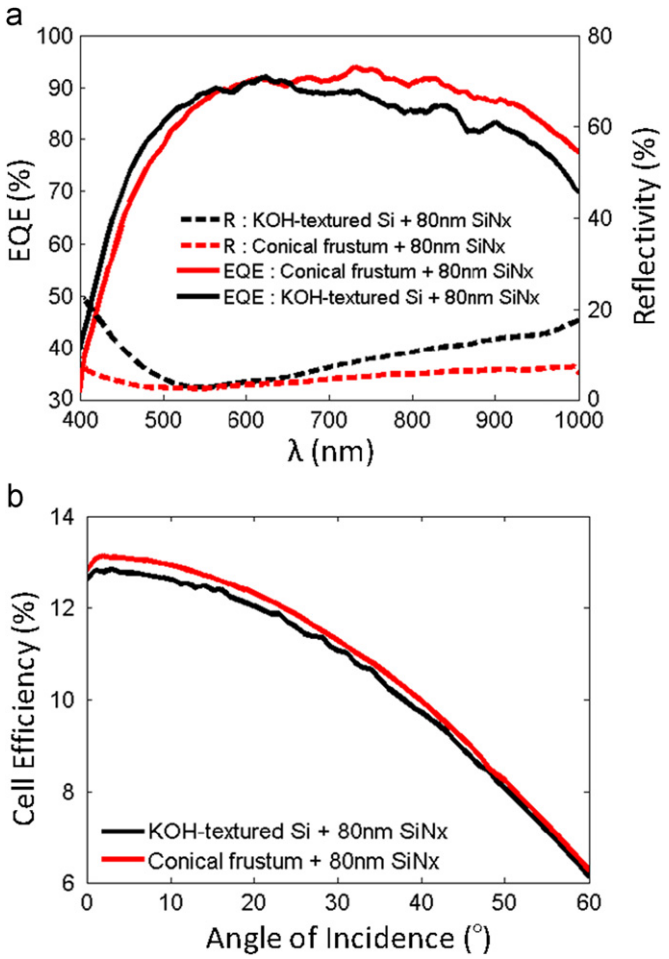

Fig. 5. (a) Measured external quantum efficiencies (EQE) and reflectivities for solar cells with the KOH-etched textures and the conical-frustum arrays, both with 80 nm-thick SiN_x. (b) The angular power conversion efficiency calculated using the measured angle-resolved reflectance spectra for both cells.

Table 1
Current–voltage characteristics of solar cells with KOH-etched textures and conical-frustum arrays, both passivated with 80 nm-thick SiN_x.

Structure	V_{oc} (V)	J_{sc} (mA/cm^2)	Fill factor (%)	Efficiency (%)
KOH-textures	0.59	29.32	70.97	12.27 ± 0.19[a]
Conical-frustum	0.59	32.46	69.82	13.39 ± 0.34[a]

[a] The statistics present the error range of six measured samples.

4. Conclusions

In summary, we demonstrated the broadband and omnidirectional antireflective characteristics of passivated conical-frustum nanostructures fabricated on crystalline silicon using polystyrene colloidal lithography. The measured cell efficiencies were improved from 12.27% for the conventional KOH-textured cell to 13.39% for the conical-frustum arrays, both with 80 nm-thick SiN_x passivation. The external quantum efficiency measurement confirmed the photocurrent enhancement contributed by the enhanced optical absorption in the near-infrared wavelength range. Furthermore, the angular efficiencies were calculated using the angle-resolved reflectance spectra. Solar cell with passivated conical-frustum arrays showed improved angular power conversion efficiencies up to an angle of incidence of 49°, promising increased current generation throughout the entire day.

Acknowledgments

This work is supported by National Science Council (NSC), Taiwan, ROC under Grant nos. NSC97-2120-M-006-009 and NSC96-2628-E009-017-MY3.

References

[1] P. Lalanne, G.M. Morris, Design, fabrication and characterization of subwavelength periodic structures for semiconductor anti-reflection coating in the visible domain, Proc. SPIE 2776 (1996) 300.
[2] C.C. Striemer, P.M. Fauchet, Dynamic etching of silicon for broadband antireflection applications, Appl. Phys. Lett. 81 (2002) 2980.
[3] C.H. Sun, P. Jiang, B. Jiang, Broadband moth-eye antireflection coatings on silicon, Appl. Phys. Lett. 92 (2008) 061112.
[4] M. Tao, W. Zhou, H. Yang, L. Chen, Surface texturing by solution deposition for omnidirectional antireflection, Appl. Phys. Lett. 91 (2007) 081118.
[5] Y. Kanamori, M. Sasaki, K. Hane, Broadband antireflection gratings fabricated upon silicon substrates, Opt. Lett. 24 (1999) 1422–1424.
[6] C.H. Sun, B.J. Ho, B. Jiang, P. Jiang, Biomimetic subwavelength antireflective gratings on GaAs, Opt. Lett. 33 (2008) 2224–2226.
[7] H. Sai, H. Fujii, K. Arafune, Y. Ohshita, Y. Kanamori, H. Yugami, M. Yamaguchi, Wide-angle antireflection effect of subwavelength structures for solar cells, Jpn. J. Appl. Phys. Part 1 46 (2007) 3333.
[8] H. Sai, Y. Kanamori, K. Arafune, Y. Ohshita, M. Yamaguchi, Light trapping effect of submicron surface textures in crystalline Si solar cells, Prog. Photovoltaics 15 (2007) 415.
[9] H.M. Wu, C.M. Lai, L.H. Peng, Optical response from lenslike semiconductor nipple arrays, Appl. Phys. Lett. 93 (2008) 211903.
[10] Y.F. Huang, S. Chattopadhyay, Y.J. Jen, C.Y. Peng, T.A. Liu, Y.K. Hsu, C.L. Pan, H.C. Lo, C.H. Hsu, Y.H. Chang, C.S. Lee, K.H. Chen, L.C. Chen, Improved broadband and quasi omnidirectional antireflection properties with biomimetic silicon nanostructures, Nat. Nanotechnol. 2 (2007) 770–774.
[11] D.S. Hobbs, B.D. MacLeod, J.R. Riccobono, Update on the development of high performance antireflection surface relief micro-structures, Proc. SPIE 6545 (2007) (65450Y-1-14).
[12] C.H. Chiu, P. Yu, H.C. Kuo, C.C. Chen, T.C. Lu, S.C. Wang, S.H. Hsu, Y.J. Cheng, Y.C. Chang, Broadband and omnidirectional antireflection employing disordered GaN nanopillars, Opt. Express 16 (2008) 8748–8754.
[13] W.L. Min, B. Jiang, P. Jiang, Bioinspired self-cleaning antireflection coatings, Adv. Mater. 20 (2008) 3914–3918.
[14] A.R. Parker, H.E. Townley, Biomimetics of photonic nanostructures, Nat. Nanotechnol. 2 (2007) 347–353.
[15] J. Schmidt, M. Kerr, A. Cuevas, Surface passivation of silicon solar cells using plasma-enhanced chemical-vapour-deposited SiN films and thin thermal SiO_2/plasma SiN stacks, Semicond. Sci. Technol. 16 (2001) 3.
[16] A.G. Aberle, Overview on SiN surface passivation of crystalline silicon solar cells, Sol. Energy Mater. Sol. Cells 65 (2001) 239–248.
[17] S.H. Lee, I. Lee, J. Yi, Silicon nitride films prepared by high-density plasma chemical vapor deposition for solar cell applications, Surf. Coat. Technol. 153 (2002) 67–71.
[18] A. El amrani, I. Menous, L. Mahiou, R. Tadjine, A. Touati, A. Lefgoum, Silicon nitride film for solar cells, Renewable Energy 33 (2008) 2289–2293.
[19] D.H. Macdonald, A. Cuevas, C. Samundsett, D. Ruby, S. Winderbaum, A. Leo, Texturing industrial multicrystalline silicon solar cells, Sol. Energy Mater. Sol. Cells 80 (2004) 227–237.
[20] H.L. Chen, S.Y. Chuang, C.H. Lin, Y.H. Lin, Using colloidal lithography to fabricate and optimize sub-wavelength pyramidal and honeycomb structures in solar cells, Opt. Express 15 (2007) 22.
[21] M.Y. Chiu, C.H. Chang, M.A. Tsai, F.Y. Chang, P. Yu, Improved optical transmission and current matching of a triple-junction solar cell utilizing sub-wavelength structures, Opt. Express 18 (2010) A308–A313.
[22] 〈http://www.samcointl.com/products/RIE-10NR.shtml〉.
[23] 〈http://www.samcointl.com/products/PD-220NL.shtml〉.
[24] ASTMG173-03, Standard Tables for Reference Solar Spectral Irradiances, ASTM International, West Conshohocken, Pennsylvania, 2005.
[25] K.A. Emery, C.R. Osterwald, Solar cell calibration methods, Sol. Cells 27 (1989) 445–453.
[26] K.A. Emery, C.R. Osterwald, T.W. Cannon, D.R. Myers , J. Burdick, T. Glatfelter, W. Czubatyj, J. Yang, Methods for measuring solar cell efficiency independent of reference cell or light source, in: Proceedings of the 18th IEEE Photovoltaic Specialists Conference, 1985, pp. 623–628.
[27] V.V. Iyengar, B.K. Nayak, M.C. Gupta, Optical properties of silicon light trapping structures for photovoltaics, Sol. Energy Mater. Sol. Cells 94 (2010) 2251–2257.
[28] D. Kumar, S.K. Srivastava, P.K. Singh, M. Husain, V. Kumar, Fabrication of silicon nanowire arrays based solar cell with improved performance. Sol. Energy Mater. Sol. Cells, in press, doi:10.1016/j.solmat.2010.04.024.